coatings

MDPI

Article

Study of the Tribological Properties of HVOF-Sprayed Ni-Based Coatings on Ti6Al4V Titanium Alloys

Pengcheng Du [1], Chang Liu [1], Hongyun Hu [2], Chunhui Zhang [3], Mingzhen Fan [1], Mingchuan Gao [1] and Tongzhou Chen [1,*]

[1] State Key Laboratory of Special Surface Protection Materials and Application Technology, Wuhan Research Institute of Materials Protection, Wuhan 430030, China
[2] State Key Laboratory of Coal Combustion, School of Energy and Power Engineering, Huazhong University of Science and Technology, Wuhan 430074, China
[3] Wuhan Marine Machinery Plant Co., Ltd., Wuhan 430084, China
* Correspondence: chentongzhou@rimp.com.cn

Abstract: In aviation, the relative sliding between titanium alloy components causes varying degrees of wear. This work aimed at reducing abrasion between titanium alloy parts and improving their service life. Three different Ni-based coatings, WC-10Ni, Ni45, and NiCr coatings, are sprayed on the surface of Ti6Al4V alloy by HVOF. Test results of the mechanical and tribological properties of such coatings show that the hardness of the Ni45 and NiCr coatings are 673 $HV_{0.1}$ and 438 $HV_{0.1}$, respectively, which are lower than that of the WC-10Ni coating. When subjected to a high load, the Ni45 and NiCr coatings suffer a cracking of flat particle interfaces due to the low hardness, which lowers the fracture toughness more than that of the WC-10Ni coating. The specific wear rates of the coatings gradually decrease with the increase in the coating hardness and fracture toughness. However, the cutting of Ti6Al4V by the WC-10Ni coating and the adhesion of the NiCr coating to Ti6Al4V result in severe wear loss of the Ti6Al4V friction pair. The moderately hard Ni45 coating has a weaker cutting and adhesion effect on Ti6Al4V than the WC-10Ni and NiCr coatings, respectively, and the Ti6Al4V friction pair has the lowest wear loss. This study is a viable scheme for the design of wear-resistant coatings on titanium alloy surfaces and for improving the tribological properties between titanium alloy components.

Keywords: HVOF; Ti6Al4V alloy; coating; hardness; fracture toughness; tribological properties

Citation: Du, P.; Liu, C.; Hu, H.; Zhang, C.; Fan, M.; Gao, M.; Chen, T. Study of the Tribological Properties of HVOF-Sprayed Ni-Based Coatings on Ti6Al4V Titanium Alloys. *Coatings* **2022**, *12*, 1977. https://doi.org/10.3390/coatings12121977

Academic Editor: Diego Martinez-Martinez

Received: 15 November 2022
Accepted: 12 December 2022
Published: 16 December 2022

1. Introduction

Titanium alloys are widely used in the aerospace, petrochemical, medical devices, and other fields due to their excellent properties such as high specific strength, corrosion resistance, fatigue resistance, and low thermal expansion coefficient [1,2]. However, titanium alloys also have the shortcomings of low hardness and poor wear resistance, which make them extremely sensitive to adhesive wear and fretting wear [3–5]. To improve the wear resistance of titanium alloy, researchers carried out surface modification of titanium alloy by plasma carbonization/nitriding, shot peening, and wear-resistant coatings [6–11]. Among these surface modification methods, the preparation of wear-resistant coatings, which have the advantage of hardness and thickness tunability, is considered to be the most effective method for enhancing the wear resistance of titanium alloys. Researchers have made many explorations in the selection of coating materials and process methods, such as preparing wear-resistant coatings by PVD or CVD [12,13], laser cladding high-entropy alloy coatings [14–16], thermal spraying coatings [17], etc.

Based on previous studies, mechanical properties play a vital role in improving the wear resistance of titanium alloys. S. Thirumalvalavan [17] sprayed SiC coatings on the surface of Ti6Al4V alloy by HVOF, and the surface hardness was increased from 303 HV to 756 HV. The surface wear resistance was found to be significantly improved by friction

testing with EN31 stainless steel. Pawlak [12] deposited a WC_{1-x}/C film on the surface of Ti6Al4V titanium alloy, the surface hardness was increased to 1000 HV, and the wear rate was reduced by 94%. Li [18] prepared the WC-reinforced Co-based alloy on the surface of Ti6Al4V alloy by laser cladding. The wear resistance of the coating was found to be 2–4.5 times higher than that of the titanium alloy substrate by friction with Al_2O_3. Li [19] prepared a Ni-WC coating on a commercial pure titanium grade 2 substrate by electroplating and electron beam remelting, and the surface hardness was increased to 745 HV. The results of a friction experiment using Si_3N_4 as the friction pair showed that the wear resistance of the coating was 6 times that of the substrate. CuNiIn is a solid lubricating material with a low friction coefficient and low hardness, which ensures a good interface matching between contact surfaces of the titanium alloy parts. Thermally sprayed CuNiIn coating is widely used to resist fretting wear in the case of a titanium alloy/titanium alloy contact [5,11,20]. However, owing to the low hardness of CuNiIn, such a coating suffers a large wear loss in the above-mentioned application, which can easily lead to contact between titanium alloy and titanium alloys [5,21]. In summary, there are two main surface wear resistance modification strategies for titanium alloys. One strategy is to spray a lubricating coating with low hardness, e.g., CuNiIn coating, as the soft coating can achieve the interface matching between the titanium alloy parts through its own deformation. Another strategy is to deposit a hard coating and add a self-lubricating material to reduce the coefficient of friction of the coating. This strategy has been used in mechanical components exposed to slurries such as in the oil and gas industries [22,23]. However, there is a lack of studies on the sliding tribological properties of titanium alloys in friction with protective coatings. The effect of the mechanical properties of the coating on the comprehensive wear properties of the coating–titanium alloy system should be studied.

As Ni-based coatings show a good lubricating property, in this work, three commercially available coatings, WC-10Ni, Ni45, and NiCr coatings, with high, moderate, and low hardness, respectively, were sprayed on the surface of Ti6Al4V alloy by HVOF. The effect of mechanical properties such as coating hardness and fracture toughness on the tribological properties of Ti6Al4V alloy were investigated, and the wear mechanisms of the different hardness coatings on Ti6Al4V alloy were also mastered. This work aims to provide technical support for the design and preparation of a wear-resistant coating on titanium alloy surfaces.

2. Experimental Section

2.1. Experimental Methods and Materials

The substrates for HVOF spraying experiments were Ti6Al4V alloy bars with a size of 100 mm × 25 mm × 10 mm. The substrates were cleaned with acetone, and then the surface was blasted with alumina grits size of −24~+30 mesh with a 0.5~0.6 MPa blasting pressure. WC-10Ni powders with a diameter of 15~45 μm, Ni45 powders with a diameter of 20~53 μm, and NiCr powders with a diameter of 20~53 μm, were used as feedstock materials. The composition of powder elements is shown in Table 1. A GTV K2 system on which the powders were fed into the HVOF flame with two laterally fixed inlets using N_2 as carrier gas was used as spraying equipment. The HVOF parameters are shown in Table 2.

Table 1. Chemical composition of the powders (wt %).

Element	WC	Ni	Cr	Fe	B	Si	C
WC-10Ni	90	10	-	-	-	-	-
Ni45	-	Bal.	8.00	≤10	2.0	3.5	0.05
NiCr	-	80	20	-	-	-	-

Table 2. HVOF parameters for spraying coatings.

Parameters	Value
Oxygen	950 L/min
Kerosene	24 L/h
Powder feed rate	100 g/min
Spray distance	400 mm

2.2. Microstructure and Performance Characterization

The cross-sectional morphology of the coatings was observed by using a JSM-6510LV scanning electron microscope (JEOL, Tokyo, Japan). Based on the SEM image analysis, the porosity of coatings was calculated with 5 images at a magnification of 200X according to the conventional method adopted for cemented carbide bulk material as well as coatings [24]. The phase structure was analyzed using X-ray diffraction measurement with Cu Kα radiation on a SHIMADZU XRD-600 diffractometer (Shimadzu, Kyoto, Japan).

The coating microhardness was measured at 0.98 N load with 15 s dwelling time, on the cross-section of coatings using a TMVS-1 Vickers indentation tester (Beijing Era's Peak Technology Co., Beijing, China), and each value was averaged over 10 measurements. The coating fracture toughness was obtained by Equation (1), employing a Vickers indentation method under a load of 49 N [25], in which the equation should satisfy $0.6 < c/a < 4.5$.

$$K_{IC} = 0.079P/a^{3/2}\log(4.5a/c) \quad (1)$$

where P is the indention load, a the average half-length of indentation size, and c the averaged half-length of the crack extended along the indent diagonal.

The tribological properties of Ti6Al4V friction pair pressured against block coating samples were tested using Rtec MFT-5000 wear testing machine (Rtec Instruments, City of San Jose, CA, USA). The coating and the Ti6Al4V friction pair are ground and polished to a surface roughness R_z 0.8–1.5 μm before testing. The friction test diagram is shown in Figure 1. The Ti6Al4V friction pair and coatings formed plane/plane contact at a load of 100 N, and the friction process lasted for 30 min with a sliding distance of 4 mm at a frequency of 2 Hz.

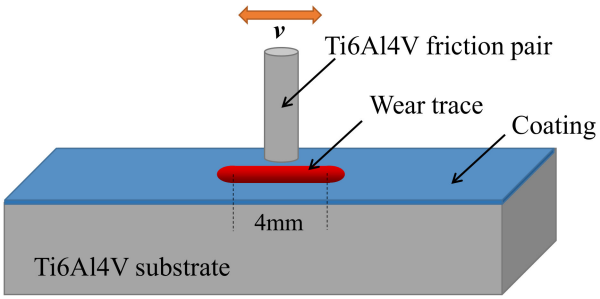

Figure 1. Friction test diagram.

The morphology and depth of the coating wear trace were analyzed by a white light confocal 3D morphology tester (Sciences et Techniques Industrielles de la Lumière, Aix-en-Province, France), and the weight loss of the Ti6Al4V friction pair was measured as well. Mitutoyo SJ-210 surface roughness tester (Mitutoyo, Kanagawa, Japan) was used to measure the surface roughness of coating wear traces and Ti6Al4V friction pairs, in which the test direction was perpendicular to the direction of friction motion. The coating specific wear rate was obtained by Equation (2), in which the volume of wear trace was integrated via Origin software:

$$\omega = \frac{V}{f \times s \times t \times F} \quad (2)$$

where V is the wear volume, f the sliding frequency, t the test time, s the sliding distance for one trace, and F the pressure load.

3. Results and Discussion

3.1. Coating Microstructure

Figure 2 shows the cross-section of WC-10Ni, Ni45, and NiCr coatings. It can be seen from the 200× macro morphology of the coating that all the coatings have a dense structure with a thickness of about 350 μm, and the porosity of the Ni45 coating is slightly higher than that of the WC-10Ni and the NiCr coatings. All the coatings are free of cracks or other imperfections and are tightly bonded to the substrate. From Figure 2b, WC-10Ni coating shows a dense structure without obvious pore or stratification features, in which WC hard particles are uniformly distributed. The Ni45 coating is distributed with pores in a diameter of 1–3 μm, similar to other HVOF-sprayed NiCrBSi coatings [26]. The cross-section morphology of the NiCr coating is shown in Figure 2f. It can be seen that the microstructure of the NiCr coating is dense without obvious pores and features of a flattened particle interface.

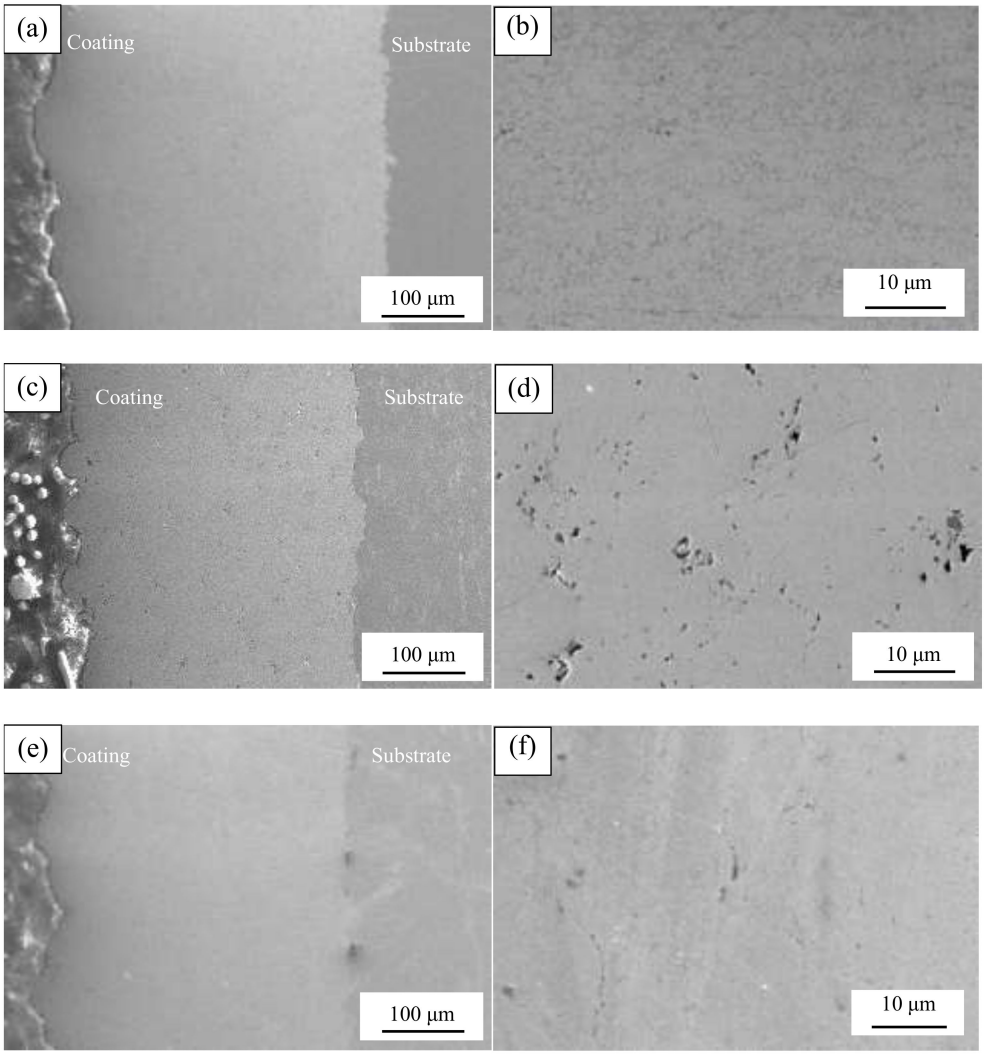

Figure 2. Cross-section morphology of the coatings: (**a**,**b**) WC-10Ni; (**c**,**d**) Ni45; (**e**,**f**) NiCr.

Figure 3 shows the porosity and surface roughness, R_z, of the coatings. The porosity values of the WC-10Ni, Ni45, and NiCr coatings sprayed with the same parameters are 0.78%, 1.03%, and 0.63%, respectively, and the corresponding surface roughness values,

R_z, are 23.4 μm, 43.2 μm, and 52.7 μm. The porosity of the coatings is determined by the spraying process and parameters, powder material, and particle size [27]. Table 3 shows the melting point of raw materials. In this study, the NiCr powders were found to melt better than the WC-Ni powders, resulting in a lower porosity, as the coatings were sprayed with the same parameters. Other related studies have shown that the NiCr coating sprayed by HVOF has a denser structure than WC coatings [28,29].

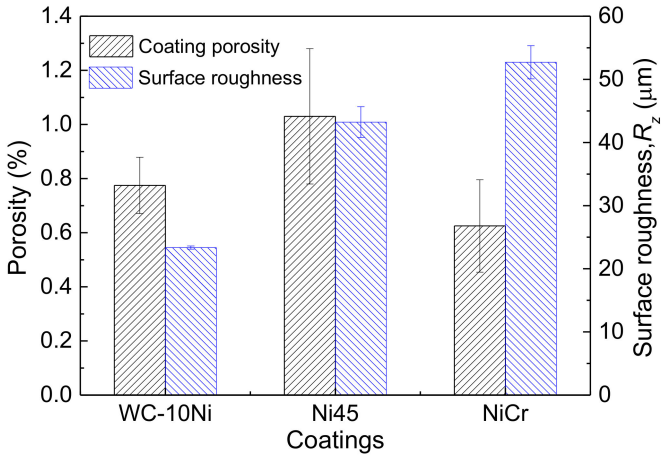

Figure 3. The coating porosity and surface roughness.

Table 3. The melting point of raw materials.

Raw Materials	Ni	Ni20%Cr	NiCrBSi	WC
Melting point/°C	1453 [30]	1400 [31]	993 [31]	2750 [32]

As shown in Table 1, the Ni content in Ni45 powder is close to that in the NiCr coating. In addition, the addition of B, Si, and other elements can reduce the melting point of the powder [31,33]. The melting point of NiCrBSi is about 993 °C, which is lower than that of NiCr at 1400 °C, so the Ni45 sprayed particles have a higher melting degree than NiCr particles. However, the porosity of the Ni45 coating is significantly higher than that of the WC-10Ni coating and NiCr coatings. The reason may be that the Cr, C, and B in the molten Ni45 particles reacted to form a hard phase and amorphous phase during the thermal spraying process [33,34], which eventually led to a decrease in the temperature and an increase in the viscosity of molten particles. The surface oxidation of sprayed particles and the hardening caused by cooling resulted in more obvious pores in the Ni45 coating than in the NiCr coating [35]. Meanwhile, the Ni45 particles lack hard particles such as those in the WC-10Ni coating, and the particle kinetic energy is lower than that of WC-10Ni, resulting in a higher porosity of the coatings than that of WC-10Ni. Wang et al. [36] studied the morphology of NiCrBSi and WC-Co particles sprayed by HVOF and found that NiCrBSi particles have a better spreading property, which leads to easier splashing of particles on the deposited surface and an increase in the surface roughness. The surface roughness of a flame-sprayed NiCrBSi coating is higher than that of the NiCrBSi-WC coating and the surface roughness of the HVOF-sprayed cobalt-based alloy is higher than that of the WC-Co coating, which can also prove that the deposition process of metal particles is more likely to cause the particle to spatter [37,38]. This is also the reason why the surface roughness of the NiCr coating sprayed by HVOF is higher than that of the WC-Co coating [28].

3.2. The Phase Structure

Figure 4 shows the XRD patterns of the powders and coatings. It can be seen from Figure 4a that there are only the WC phase and Ni phase in the powders, while the W_2C and WC_{1-X} phases are detected in the coating, indicating that WC particles are oxidized

in the spraying process. The decomposition of WC is common in the process of thermal spraying and can lead to a reduction in hardness and fracture toughness [39,40]. It can be seen from Figure 4b that the Ni45 powder and coating mainly consists of γ-Ni, and other hard ceramic phases such as $Cr_{23}C_6$, Cr_7C_3, and CrB [30]. Because the spray particles stay in the supersonic flame for a short time, the phase structure of the coating has no obvious change compared with the powder. Figure 4c shows the XRD patterns of the NiCr powders and coating. The dominant phase of the NiCr powder and coating is γ-Ni, which is consistent with the results in [28].

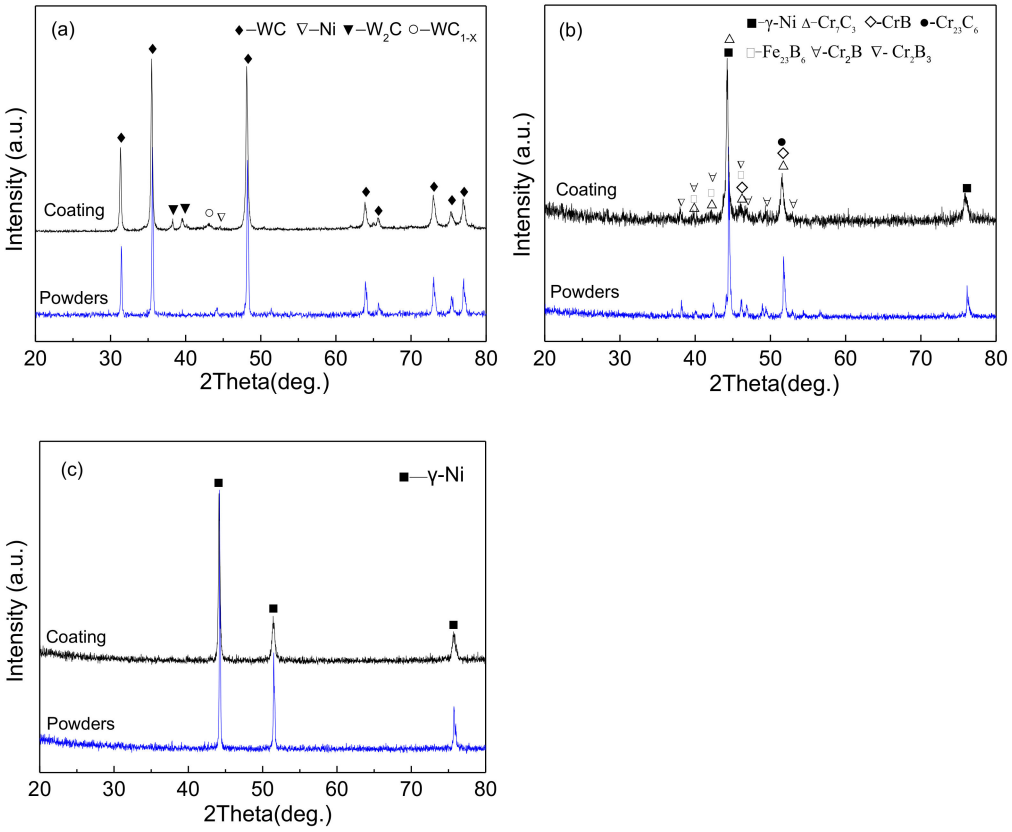

Figure 4. XRD patterns of the powders and coatings: (**a**) WC-10Ni; (**b**) Ni45; (**c**) NiCr.

3.3. Coating Mechanical Properties

Figure 5 shows the microhardness and fracture toughness of the coating and Ti6Al4V alloy obtained by the indentation method. The microhardness of the Ti6Al4V alloy is about 314 $HV_{0.1}$, while those of the WC-10Ni, Ni45, and NiCr coatings are 1156 $HV_{0.1}$, 673 $HV_{0.1}$, and 438 $HV_{0.1}$, respectively. The fracture toughness of WC-10Ni, Ni45, and NiCr coatings are calculated by Equation (1). According to the data shown in Figure 4, the WC-10Ni coating with the highest hardness also has the highest fracture toughness of 4.66 $Mpa \cdot m^{1/2}$; the Ni45 coating with the middle hardness has the middle fracture toughness of about 3.43 $Mpa \cdot m^{1/2}$, and the NiCr coating has the lowest fracture toughness of 1.69 $Mpa \cdot m^{1/2}$.

Figure 6 shows the indentation morphology of WC-10Ni, Ni45, and NiCr coatings at 49 N load. The cracks in the WC-10Ni coating are generated at the sharp corners of the indentation in the transverse direction and propagate along the direction parallel to the interface. The cracks are generated in the stress concentration area at the indentation tip and propagate along the structures such as pores, interparticle interfaces, and rich adhesive phase areas, which are the weak sites for coating bonding [39]. Since Ni45 and NiCr coatings have a lower hardness than WC-10Ni coatings, they are subject to a stronger pinching and pulling effect by the indenter. In addition to the cracks in the stress concentration

region at the tip of the indentation, the microcracks around the indentation are caused by interparticle interface cracking.

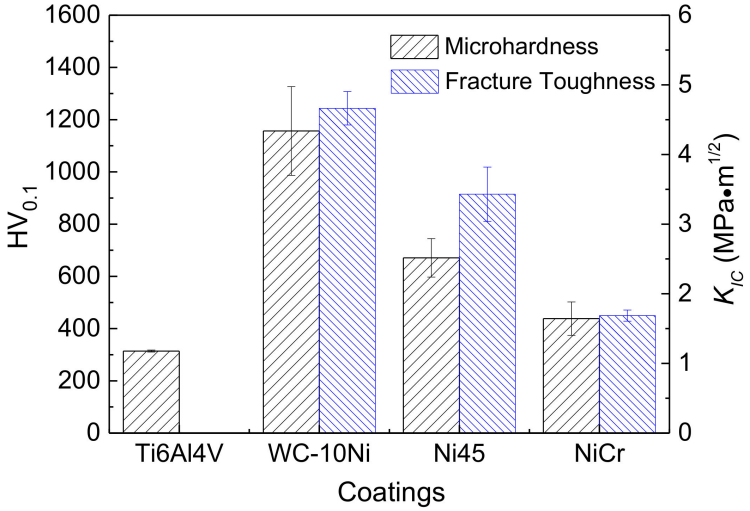

Figure 5. Microhardness and fracture toughness of the coatings.

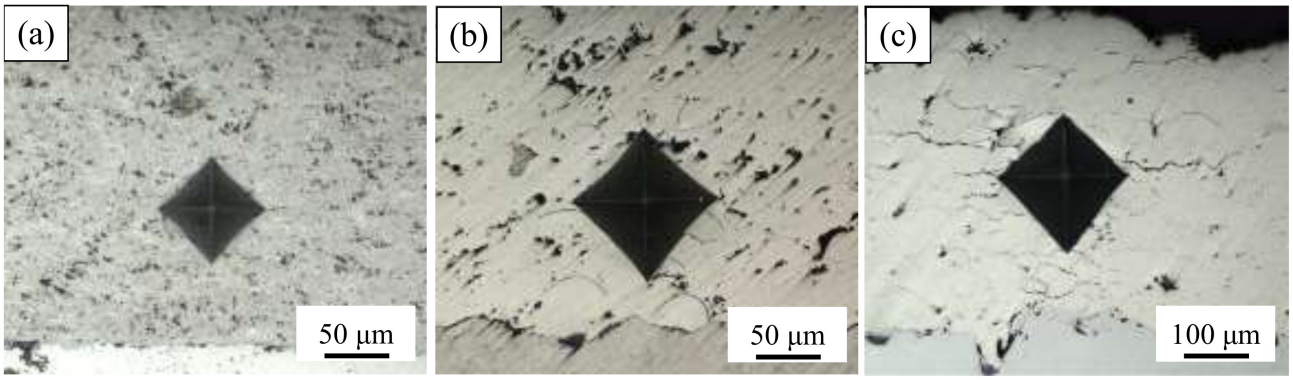

Figure 6. Indentation morphology of the coatings: (**a**) WC-10Ni, (**b**) Ni45, (**c**) NiCr.

3.4. Tribology Properties of Coatings in Friction with Ti6Al4V

3.4.1. Friction Coefficient

Figure 7 shows the friction coefficient curves of Ti6Al4V pressured on Ti6Al4V substrate and different coatings. The friction coefficients in different cases are almost the same in the first 200 s of the wear test, which is defined as the running-in stage. After this stage, the Ti6Al4V friction pair had already gotten in full contact with the coating, so the friction coefficients started to show significant differences. The mean values of the friction coefficients show that the Ti6Al4V/Ti6Al4V friction had the lowest friction coefficient of 0.34 ± 0.047. The friction coefficient between the coating and the Ti6Al4V frictional pair is larger than the Ti6Al4V/Ti6Al4V frictional pair. The average friction coefficients between the WC-10Ni, Ni45, and NiCr coatings and the Ti6Al4V friction pair were about 0.39 ± 0.056, 0.40 ± 0.054, and 0.44 ± 0.081, respectively. Ti6Al4V/Ti6Al4V friction shows the mildest friction coefficient curves, while NiCr/Ti6Al4V friction shows the largest friction coefficient fluctuations.

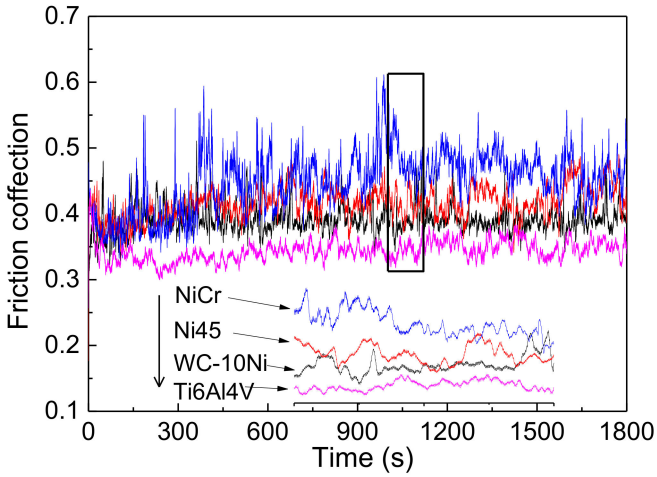

Figure 7. Friction coefficient of Ti6Al4V alloy and coatings.

3.4.2. Wear Loss

Figure 8 shows the wear profile obtained by SPIP optical analysis software. It can be seen that the wear width and depth of the NiCr coating are significantly higher than those of the Ti6Al4V substrate, Ni45 coating, and NiCr coating, and the wear traces show deeper furrow-cut features. Although the wear depth of Ti6Al4V alloy is lower than that of the NiCr coatings, the wear traces still show more pronounced furrow-cut features than those of the WC-10Ni and Ni45 coatings. The WC-10Ni coating shows the smallest abrasion depth; that is, it has the smallest wear volume.

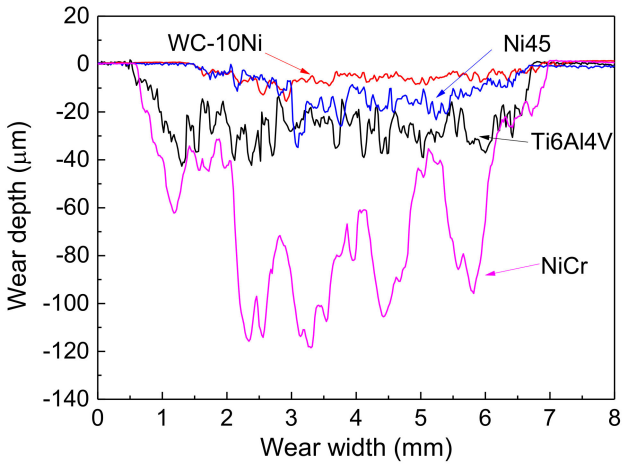

Figure 8. Cross-sectional wear trace of Ti6Al4V alloy and coatings.

Three sets of coatings as well as Ti6Al4V friction pairs were used to analyze the wear loss and the wear trace surface roughness. Figure 9 shows the surface roughness of the coating and the Ti6Al4V friction pair. In general, the surface roughness R_z of the coating corresponded with the wear trace profile curves of that coating as shown in Figure 8; that is, the coating with larger furrow cuttings had a larger roughness. The wear trace surface roughness values of the Ti6Al4V substrate, WC-10Ni coating, Ni45 coating, and NiCr coating were about 22.9 μm, 9.5 μm, 14.9 μm, and 38.2 μm, while the corresponding wear trace roughness values of the Ti6Al4V friction pair were 21.8 μm, 15.5 μm, 20.2 μm, and 35.7 μm, respectively. Since the Ti6Al4V substrate and the friction pair are made of the same material, they show almost the same value of the wear trace roughness, and the friction pair in the friction with the Ni45 coating shows the same roughness as the friction pair in the friction with the Ti6Al4V substrate.

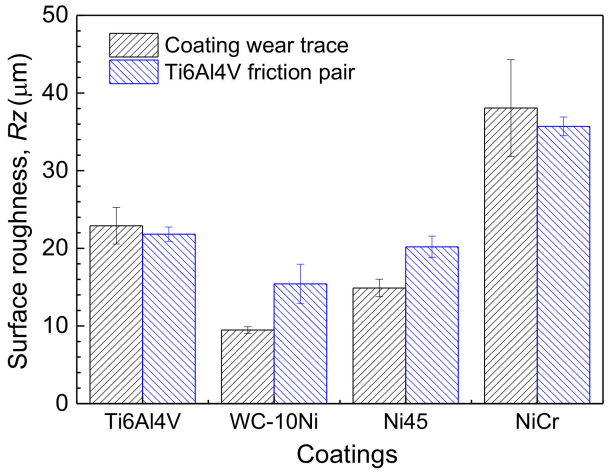

Figure 9. Wear trace roughness of the coatings and Ti6Al4V friction pair.

Figure 10 shows the specific wear rates and wear loss of the coatings and the Ti6Al4V alloy, in which the specific wear rates are calculated by Equation (2). The specific wear rate of the coating increased with the decrease in coating hardness. The specific wear rates of the WC-10Ni, Ni45, and NiCr coatings are 0.93×10^{-7} mm^3/(N·m), 1.83×10^{-7} mm^3/(N·m), and 11.4×10^{-7} mm^3/(N·m), respectively. The specific wear rate of the Ti6Al4V alloy substrate is about 4.3×10^{-7} mm^3/(N·m), which is almost 4.6 times and 2.3 times that of the WC-10Ni and Ni45 coatings, respectively, and much lower than that of the NiCr coating. There is no linear relationship between the wear loss of the Ti6Al4V friction pair and the coating hardness. The Ti6Al4V friction pair has a wear loss of 2.54 mg, 8.43 mg, 2.74 mg, and 69.97 mg, respectively, on friction with the Ti6Al4V substrate, WC-10Ni coating, Ni45 coating, and NiCr coating. It can be seen from the above data that the wear loss of the Ti6Al4V friction pair in Ti6Al4V/Ti6Al4V friction is close to that in the Ni45 coating/Ti6Al4V friction, and lower than that in friction with the WC-10Ni and NiCr coatings, meaning that Ti6Al4V has the lowest wear loss in friction with the Ni45 coating with moderate hardness. Ni45/Ti6Al4V has the best comprehensive wear performance.

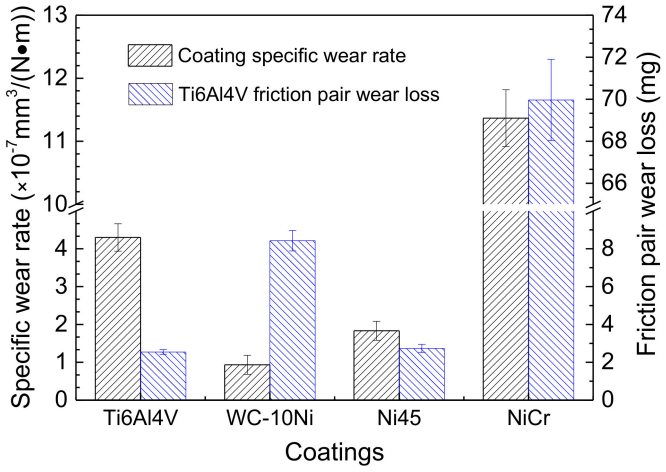

Figure 10. The specific wear rate of the coatings and the wear loss of the Ti6Al4V friction pair.

3.4.3. Wear Morphology and Wear Mechanism

Figure 11 shows the wear trace morphology of the coatings and the Ti6Al4V friction pair. It can be seen from Figure 11a,b that the Ti6Al4V substrate and Ti6Al4V friction pair show the same wear trace morphology with obvious fluctuations and furrow cuttings features on the wear trace surface. Although the substrate and friction pair are polished, the surface of the material still has fluctuation features. During the friction process, the Ti6Al4V

alloy deforms and bites together under the normal load first, and then the small material particles fall off to form abrasive particles under the shear load due to the adhesion between the substrate and friction pair [41]. As a result, deep and uniform furrow cuttings are produced on the surfaces of the substrate and the friction pair. In this case, both the Ti6Al4V substrate and friction pair show an adhesive and abrasive mixed wear mechanism, which is in accordance with previous studies of sliding tribological properties of Ti6Al4V [42].

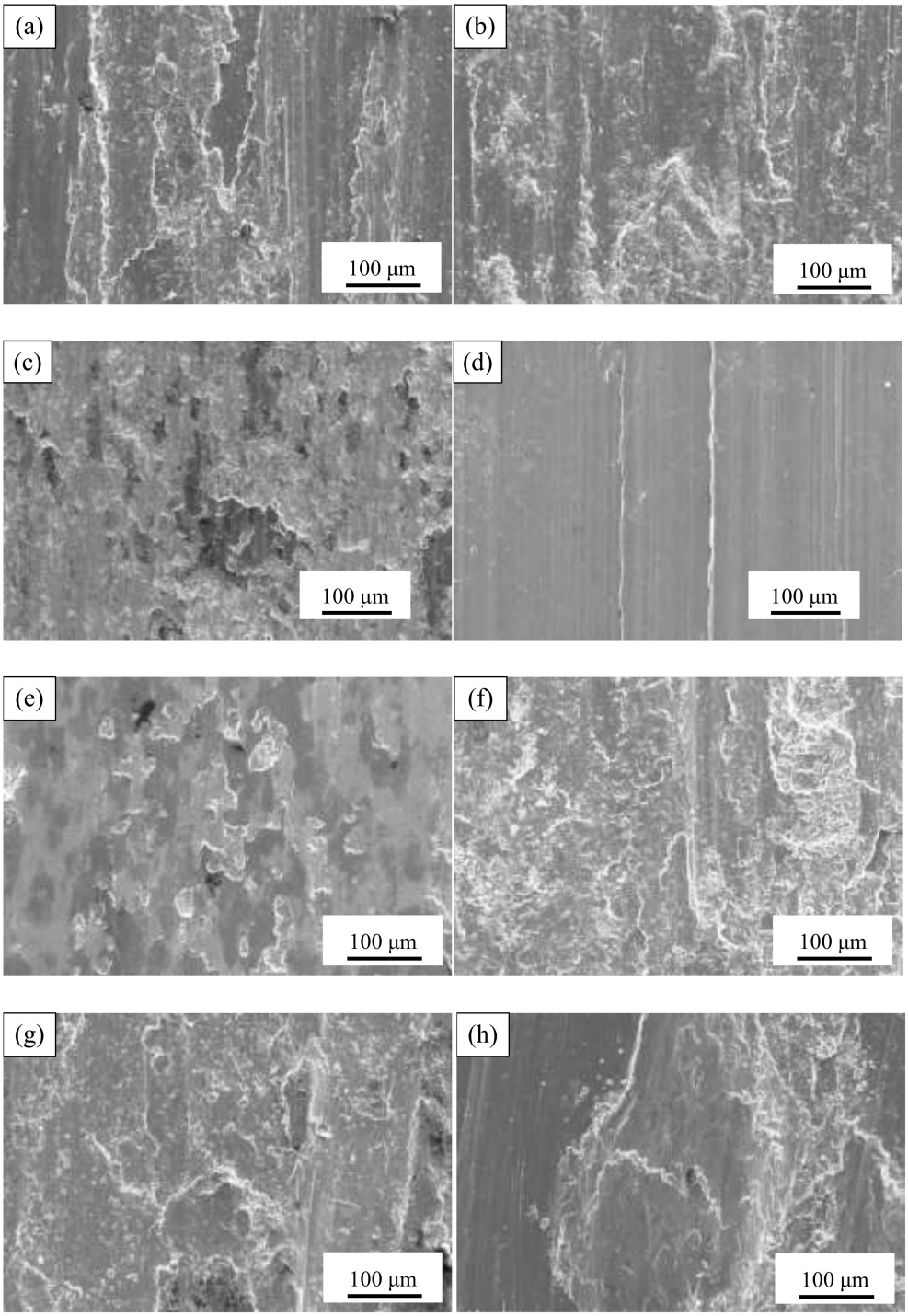

Figure 11. Surface wear trace micrographs: (**a**,**b**) Ti6Al4V substrate and Ti6Al4V friction pair; (**c**,**d**) WC-10Ni and Ti6Al4V friction pair; (**e**,**f**) Ni45 and Ti6Al4V friction pair; (**g**,**h**) NiCr and Ti6Al4V friction pair.

Figure 11c,d show the wear morphology of the WC-10Ni coating and the Ti6Al4V friction pair. It can be seen that the surface of the WC-10Ni coating has some wear debris piled up, while the wear trace morphology of the Ti6Al4V frictional pair shows furrow-cut features with different depths and widths. As the WC-10Ni coating had a higher hardness than Ti6Al4V alloy, the high hardness "bulges" of the WC-10Ni coating have a serious cutting effect on the friction pair, resulting in severe abrasive wear of the friction, which is the main reason for the large wear loss and high wear trace surface roughness of the friction pair. It appears that the adhesion between the Ti6Al4V alloy and the Ni binding phase of the coating results in the wear of the Ni binding phase and thus causes the WC hard particles to peel off, leading to slight abrasive wear of the WC-10Ni coating. However, as the WC-10Ni coating had a high fracture toughness, the friction could hardly cause a large area of particles to peel off [40], and that is the main reason for its low wear loss and low surface roughness.

Figure 11e,f show the wear trace morphology of the Ni45 coating and the Ti6Al4V friction pair. The wear surface of the Ni45 coating shows the adhesion of abrasive debris and the breakage and peeling of the particles, which is the same as the case in other HVOF-sprayed NiCrBSi wear morphology [43,44]. Due to the low fracture toughness of the Ni45 coating as shown in Figure 5b, cracks are prone to form between particles at a large load, and then spall off from the surface of the coating under shear stress. The particle spalling features are observed from the cross-section of the wear trace in other studies [43]. The stripped hard granules then exert a cutting effect on the friction pair, and as a result, the cutting effect of the stripped hard granules leads to the formation of furrows on the friction pair surface and an increase in the surface roughness. Although the ejected particles of the Ni45 coating have a cutting effect on the Ti6Al4V frictional pair, the abrasion roughness of the latter is comparable to that of the frictional Ti6Al4V substrate. The cutting effect of Ni45 on the friction pairs is reduced due to the lower hardness compared to the WC-10Ni coating, resulting in a lower wear loss for the frictional pairs compared to the friction with the WC-10Ni coating.

Figure 11g,h show the wear morphology of the NiCr coating and Ti6Al4V alloy friction pair. Wear traces of NiCr coatings with severe interlaminar spallation show more pronounced adhesive and abrasive wear features than those of Ti6Al4V substrates. The hardness of the NiCr coating is higher than that of the Ti6Al4V alloy; however, the fracture toughness is even lower than that of the Ni45 coating, so that the NiCr particles are more likely to peel off from the substrate surface under normal and shear loads to form abrasive particles. Meanwhile, the strong adhesive effect between the NiCr coating and the friction pair results in a higher friction coefficient than that in friction with the WC-10Ni and Ni45 coatings, leading to a severe adhesive and abrasive wear of the Ti6Al4V alloy friction pair. The surface roughness and wear weight loss of the coating and the friction pair are much higher than those in the friction between the friction pair and other coating materials.

4. Conclusions

Ni-based coatings of different hardnesses were sprayed on Ti6Al4V by HVOF, and the tribological properties of the Ti6Al4V friction pair in friction with the coatings were investigated. The main conclusions of this paper are as follows.

(1) The HVOF-sprayed WC-10Ni, NiCr, and Ni45 coatings show a dense structure with a porosity of the former two lower than 1% and the last one of about 1.03%. The Ni45 and NiCr coatings have weaker bearing capacity due to their lower hardness, and their fracture toughness was also lower, only 3.43 Mpa·$m^{1/2}$ and 1.69 Mpa·$m^{1/2}$, respectively.

(2) The wear mechanism between Ti6Al4V and Ti6Al4V, as well as between the NiCr coating and Ti6Al4V, is a mixed one consisting of both adhesive and abrasive wear, which results in a great wear loss. The cutting effect of the high hardness WC-10Ni coating on the Ti6Al4V is significant, resulting in a larger wear loss of the titanium alloy. The moderate hardness Ni45 coating has a lower cutting effect on the friction pair than the WC-10Ni

coating and a lower adhesion effect than the Ti6Al4V and NiCr coatings, resulting in the lowest wear loss on the frictional pairs.

(3) Preparing a moderate hardness Ni45 coating on the surface of Ti6Al4V alloy can reduce the adhesive wear loss of the titanium alloy substrate and friction pair; thus, it can offer good surface protection for titanium alloy parts.

Author Contributions: Conceptualization; investigation, writing—original draft preparation, writing—review and editing, P.D.; methodology, C.Z.; data curation,; software, validation, C.L. and M.F.; formal analysis, M.F.; resources, H.H.; visualization, M.G.; supervision; project administration; funding acquisition, T.C. All authors have read and agreed to the published version of the manuscript.

Funding: This work is supported by the Foundation of State Key Laboratory of Coal Combustion, No. FSKLCCA1901.

Institutional Review Board Statement: Not applicable.

Informed Consent Statement: Not applicable.

Data Availability Statement: All data that support the findings of this study are included within the article.

Acknowledgments: The authors are grateful to H.T. Duan and Y.H. Li for their helpful discussion and technical assistance on the abrasion test.

Conflicts of Interest: The authors declare no conflict of interest.

References

1. Zhang, W.; Li, W.; Zhai, H.; Wu, Y.; Wang, S.; Liang, G.; Wood, R.J.K. Microstructure and tribological properties of laser in-situ synthesized Ti_3Al composite coating on Ti-6Al-4V. *Surf. Coat. Technol.* **2020**, *395*, 125944. [CrossRef]
2. Xu, G.; Shen, X. Fabrication of SiO_2 nanoparticles incorporated coating onto titanium substrates by the micro-arc oxidation to improve the wear resistance. *Surf. Coat. Technol.* **2019**, *364*, 180–186. [CrossRef]
3. Yuan, S.; Lin, N.M.; Zou, J.J.; Lin, X.Z.; Liu, Z.Q.; Yu, Y.; Wang, Z.X.; Zeng, Q.F.; Chen, W.G.; Tian, L.H.; et al. In-situ fabrication of gradient titanium oxide ceramic coating on laser surface textured Ti6Al4V alloy with improved mechanical property and wear performance. *Vacuum* **2020**, *176*, 109327. [CrossRef]
4. Ma, A.; Liu, D.X.; Tang, C.B.; Zhang, X.H.; Liu, C.S. Influence of glow plasma Co-based alloying layer on sliding wear and fretting wear resistance of titanium alloy. *Tribol. Int.* **2018**, *12*, 85–94. [CrossRef]
5. Mary, C.; Fouvry, S.; Martin, J.M.; Bonnet, B. Pressure and temperature effects on fretting wear damage of a Cu-Ni-In plasma coating versus Ti17 titanium alloy contact. *Wear* **2011**, *272*, 18–37. [CrossRef]
6. Bansal, D.G.; Eryilmaz, O.L.; Blau, P.J. Surface engineering to improve the durability and lubricity of Ti-6Al-4V alloy. *Wear* **2011**, *271*, 2006–2015. [CrossRef]
7. Ananth, M.P.; Ramesh, R. Sliding wear characteristics of solid lubricant coating on titanium alloy surface modified by laser texturing and ternary hard coatings. *T. Nonferr. Metal. Soc.China* **2017**, *27*, 839–847. [CrossRef]
8. Park, Y.G.; Wey, M.Y.; Hong, S.I. Enhanced wear and fatigue properties of Ti-6Al-4V alloy modified by plasma carburizing/CrN coating. *J Mater Sci. Mater Med.* **2007**, *18*, 925–931. [CrossRef]
9. Friedrich, V.; Fouvry, S.; Kapsa, P. Effect of shot peening on the fretting wear of Ti-6Al-4V. *Wear* **2001**, *250*, 642–649. [CrossRef]
10. Karaoglanli, A.C. Effect of severe air-blast shot peening on the wear characteristics of CP titanium. *Mater. Tehnol.* **2015**, *49*, 253–258. [CrossRef]
11. Ma, A.; Liu, D.X.; Zhang, X.H.; He, G.Y.; Liu, D.; Liu, C.S.; Xu, X.C. The fretting fatigue performance of Ti-6Al-4V alloy influenced by microstructure of CuNiIn coating prepared via thermal spraying. *Tribol. Int.* **2020**, *145*, 106156. [CrossRef]
12. Pawlak, W.; Kubiak, K.J.; Wendler, B.G.; Mathiac, T.G. Wear resistant multilayer nanocomposite WC_{1-x}/C coating on Ti-6Al-4V titanium alloy. *Tribol. Int.* **2015**, *82*, 400–406. [CrossRef]
13. Łępicka, M.; Grądzka-Dahlke, M.; Pieniak, D.; Pasierbiewicz, K.; Kryńska, K.; Niewczas, A. Tribological performance of titanium nitride coatings: A comparative study on TiN-coated stainless steel and titanium alloy. *Wear* **2019**, *422*, 68–80. [CrossRef]
14. Yang, Y.L.; Zhang, D.; Yan, W.; Zheng, Y.R. Microstructure and wear properties of TiCN/Ti coatings on titanium alloy by laser cladding. *Opt. Laser Eng.* **2010**, *48*, 119–124. [CrossRef]
15. Santecchia, E.; Hamouda, A.M.S.; Musharavati, F.; Zalnezhad, E.; Cabibbo, M.; Stefano, S. Wear resistance investigation of titanium nitride-based coatings. *Ceram. Int.* **2015**, *41*, 10349–10379. [CrossRef]
16. Xiang, K.; Chen, L.Y.; Chai, L.J.; Guo, N.; Wang, N.; Wang, H. Microstructural characteristics and properties of CoCrFeNiNbx high-entropy alloy coatings on pure titanium substrate by pulsed laser cladding. *Appl. Surf. Sci.* **2020**, *517*, 146214. [CrossRef]

17. Thirumalvalavan, S.; Senthilkumar, N.; Perumal, G.; Anantha, P.M.R. Ameliorating the wear defiance of HVOF thermal spray silicon carbide coated Ti-6Al-4V alloy using PCA-GRA technique. *Silicon* **2022**, *14*, 3101–3117. [CrossRef]
18. Li, W.; Xu, P.Q.; Wang, Y.Y.; Zou, Y.; Gong, H.Y.; Lu, F.G. Laser synthesis and microstructure of micro-and nano-structured WC reinforced Co-based cladding layers on titanium alloy. *J. Alloy. Compd.* **2018**, *749*, 10–22. [CrossRef]
19. Li, Y.S.; Song, P.; Wang, W.Q.; Lei, M.; Li, X.W. Microstructure and wear resistance of a Ni-WC composite coating on titanium grade 2 obtained by electroplating and electron beam remelting. *Mater. Charact.* **2020**, *170*, 110674. [CrossRef]
20. Niu, Z.Q.; Zhou, W.L.; Wang, C.L.; Cao, Z.W.; Yang, Q.; Fu, X.S. Fretting wear mechanism of plasma-sprayed CuNiIn coating on Ti-6Al-4V substrate under plane/plane contact. *Surf. Coat. Tech.* **2021**, *408*, 126794. [CrossRef]
21. Freimanis, A.J.; Segall, A.E.; Conway, J.C.; Whitney, E.J. Elevated temperature evaluation of fretting and metal transfer between coated titanium components. *Tribol. T.* **2000**, *43*, 653–658. [CrossRef]
22. Zaghloul, M.M.Y.; Steel, K.; Veidt, M.; Heitzmann, M.T. Wear behaviour of polymeric materials reinforced with man-made fibres: A comprehensive review about fibre volume fraction influence on wear performance. *J Reinf. Plast. Comp.* **2022**, *41*, 215–241. [CrossRef]
23. Zaghloul, M.Y.M.; Zaghloul, M.M.Y.; Zaghloul, M.M.Y. Developments in polyester composite materials–An in-depth review on natural fibres and nano fillers. *Compos Struct.* **2021**, *278*, 114698. [CrossRef]
24. Deshpande, S.; Kulkarni, A.; Sampath, S.; Herman, H. Application of image analysis for characterization of porosity in thermal spray coatings and correlation with small angle neutron scattering. *Surf. Coat. Technol.* **2004**, *187*, 6–16. [CrossRef]
25. Evans, A.G.; Wilshaw, T.R. Quasi-static solid particle damage in brittle solid-I. Observations analysis and implications. *Acta Metall.* **1976**, *24*, 939–956. [CrossRef]
26. Żórawski, W.; Skrzypek, S.J. Tribological properties of plasma and HVOF-sprayed NiCrBSi-Fe_2O_3 composite coatings. *Surf. Coat. Technol.* **2013**, *220*, 282–289. [CrossRef]
27. Tillmann, W.; Hussong, B.; Priggemeier, T.; Kuhnt, S.; Rudak, N.; Weinert, H. Influence of parameter variations on WC-Co splat formation in an HVOF process using a new beam-shutter device. *J. Therm. Spray Technol.* **2013**, *22*, 250–262. [CrossRef]
28. Karaoglanli, A.C.; Oge, M.; Doleker, K.M.; Hotamis, M. Comparison of tribological properties of HVOF sprayed coatings with different composition. *Surf. Coat. Technol.* **2017**, *318*, 299–308. [CrossRef]
29. Cho, T.Y.; Yoon, J.H.; Cho, J.Y.; Joo, Y.K.; Kang, J.H.; Zhang, S.H.; Chun, H.G.; Hwang, S.Y.; Kwon, S.C. Surface properties and tensile bond strength of HVOF thermal spray coatings of WC-Co powder onto the surface of 420J2 steel and the bond coats of Ni, NiCr, and Ni/NiCr. *Surf. Coat. Technol.* **2009**, *203*, 3250–3253. [CrossRef]
30. Chen, E.T.; Barnett, R.N.; Landman, U. Surface melting of Ni (110). *Phys. Rev. B* **1990**, *41*, 439. [CrossRef] [PubMed]
31. Somervuori, M.; Varis, T.; Oksa, M.; Suhonen, T.; Vuoristo, P. Comparative study on the corrosion performance of APS-, HVOF-, and HVAF-sprayed NiCr and NiCrBSi coatings in NaCl solutions. *J. Therm. Spray. Techn.* **2022**, *31*, 1597–1851. [CrossRef]
32. Dash, T.; Nayak, B.B. Preparation of WC–W_2C composites by arc plasma melting and their characterisations. *Ceram. Int.* **2013**, *39*, 3279–3292. [CrossRef]
33. Guo, H.J.; Li, B.; Lu, C.; Zhou, Q.; Jia, J.H. Effect of WC-Co content on the microstructure and properties of NiCrBSi composite coatings fabricated by supersonic plasma spraying. *J. Alloy. Compd.* **2019**, *789*, 966–975. [CrossRef]
34. Sang, P.; Chen, L.Y.; Zhao, C.H.; Wang, Z.X.; Wang, H.Y.; Lu, S.; Song, D.P.; Xu, J.H.; Zhang, L.C. Particle size-dependent microstructure, hardness and electrochemical corrosion behavior of atmospheric plasma sprayed NiCrBSi coatings. *Metals* **2019**, *9*, 1342. [CrossRef]
35. Deshpande, S.; Sampath, S.; Zhang, H. Mechanisms of oxidation and its role in microstructural evolution of metallic thermal spray coatings—Case study for Ni-Al. *Surf. Coat. Technol.* **2006**, *200*, 5395–5406. [CrossRef]
36. Wang, Y.Y.; Li, C.J.; Ohmori, A. Influence of substrate roughness on the bonding mechanisms of high velocity oxy-fuel sprayed coatings. *Thin Solid Films* **2005**, *485*, 141–147. [CrossRef]
37. Rachidi, R.; Kihel, B.; Delaunois, F. Microstructure and mechanical characterization of NiCrBSi alloy and NiCrBSi-WC composite coatings produced by flame spraying. *Mater. Sci. Eng. B.* **2019**, *241*, 13–21. [CrossRef]
38. Liu, J.; Bai, X.Q.; Chen, T.Z.; Yuan, C.Q. Effects of cobalt content on the microstructure, mechanical properties and cavitation erosion resistance of HVOF sprayed coatings. *Coatings* **2019**, *9*, 534. [CrossRef]
39. Chivavibul, P.; Watanabe, M.; Kuroda, S.; Shinoda, K. Effects of carbide size and Co content on the microstructure and mechanical properties of HVOF-sprayed WC-Co coatings. *Surf. Coat. Technol.* **2007**, *202*, 509–521. [CrossRef]
40. Zhu, X.P.; Du, P.C.; Meng, Y.; Lei, M.K.; Guo, D.M. Solution to inverse problem of manufacturing by surface modification with controllable surface integrity correlated to performance: A case study of thermally sprayed coatings for wear performance. *J. Tribol. T. ASME* **2017**, *139*, 061604. [CrossRef]
41. Long, M.; Rack, H.J. Friction and surface behavior of selected titanium alloys during reciprocating-sliding motion. *Wear* **2001**, *249*, 158–168. [CrossRef]
42. Magaziner, R.S.; Jain, V.K.; Mall, S. Investigation into the wear of Ti-6Al-4V under reciprocating sliding conditions. *Wear* **2009**, *267*, 368–373. [CrossRef]
43. Miguel, J.M.; Guilemany, J.M.; Vizcaino, S. Tribological study of NiCrBSi coating obtained by different processes. *Tribol. Int.* **2003**, *36*, 181–187. [CrossRef]
44. Xiao, J.K.; Wu, Y.Q.; Zhang, W.; Chen, J.; Wei, X.L.; Zhag, C. Microstructure, wear and corrosion behaviors of plasma sprayed NiCrBSi-Zr coating. *Surf. Coat. Technol.* **2019**, *360*, 172–180. [CrossRef]